

Vincent Taillandier · Vincent Echevin · Laurent Mortier
Jean-Luc Devenon

Controlling boundary conditions with a four-dimensional variational data-assimilation method in a non-stratified open coastal model

Received: 5 December 2002 / Accepted: 29 September 2003
© Springer-Verlag 2004

Abstract An innovative way to take the large-scale circulation influence into account in coastal primitive-equation models is explored by an inverse modelling approach. Restricted to barotropic external forcing, this work is a first step in the development of a four-dimensional variational (4DVAR) data-assimilation approach to estimate the best initial and open-boundary conditions that force a coastal model according to interior observations. This development is founded on the OPA modelling system which representation of barotropic coastal dynamics is restricted to motions of long time scales (\sim a day) due to its “rigid lid” approximation. Twin experiments are performed in an academic configuration of the Gulf of Lions (located in the northwestern Mediterranean Sea) to study the sensitivity of a remote barotropic forcing to different observational networks measuring surface currents deployed in this area. Three monitoring designs are tested for a large-scale barotropic perturbation in the hindcast mode. It is shown that the space and time distribution of observations acts on the efficiency of the 4DVAR method and then allows coarser datasets.

Keywords Coastal modelling · Open boundary condition · Data assimilation · Monitoring design

Responsible Editor: Phil Dyke

V. Taillandier
Laboratoire de Sondages Electromagnétiques de l'Environnement Terrestre, Université de Toulon-Var, La Garde, France

V. Echevin · L. Mortier
Laboratoire d'Océanographie Dynamique et de Climatologie, Université Pierre et Marie Curie, Paris, France

J.-L. Devenon (✉)
Laboratoire d'Océanologie et de Biogéochimie,
Centre d'Océanologie de Marseille,
Campus de Luminy, F-13288 Marseille Cedex 09
e-mail: devenon@com.univ-mrs.fr
Tel.: +33 491829109
Fax: +33 491826548

1 Introduction

The coastal area is rich in dynamical phenomena interacting in multiple scales and processes (Csanady 1982): the coastal currents respond to the influence of wind forcing, heat flux and freshwater discharge, the effects of land and slopes and remote influences transmitted from offshore. The latter becomes a major forcing on largely opened coastal basins, which is the case in the Gulf of Lions located in the south of France (see Fig. 1). In modelling practice, this external forcing is taken into account by the prescription of dynamical conditions along the lateral open boundaries. A commonly used methodology consists in using information on the large-scale circulation and variability from a basin model which embeds the region of interest. A large number of nesting methods – from specification/radiation (Chapman 1985; Palma and Matano 1998) to adaptive mesh systems (Blayo and Debreu 1999) – have been developed to provide conditions well suited for the open coastal model. These have been applied to storm surge modelling, e.g. in the Irish Sea (Jones and Davies 1998), and to regional modelling in the western Mediterranean Sea (Beckers et al., 1997; Echevin et al. 2001).

An alternative method is to use the available knowledge of the circulation inside the subdomain to specify these boundary conditions. The advantage of this approach is in providing information on the open-boundary conditions from observations located in the model domain rather than using only information from offshore, given by a lower-resolution basin model. The goal of this inverse approach is to obtain an estimation of the external forcing, consistent with the model dynamics (Lellouche et al. 1998) whether data come from an observational network or a large-scale model output. In the present work, the resolution method belongs to the class of variational data-assimilation methods developed for weather forecasting and extended now to a broad application field in oceanography. Its use in estimating open boundary conditions

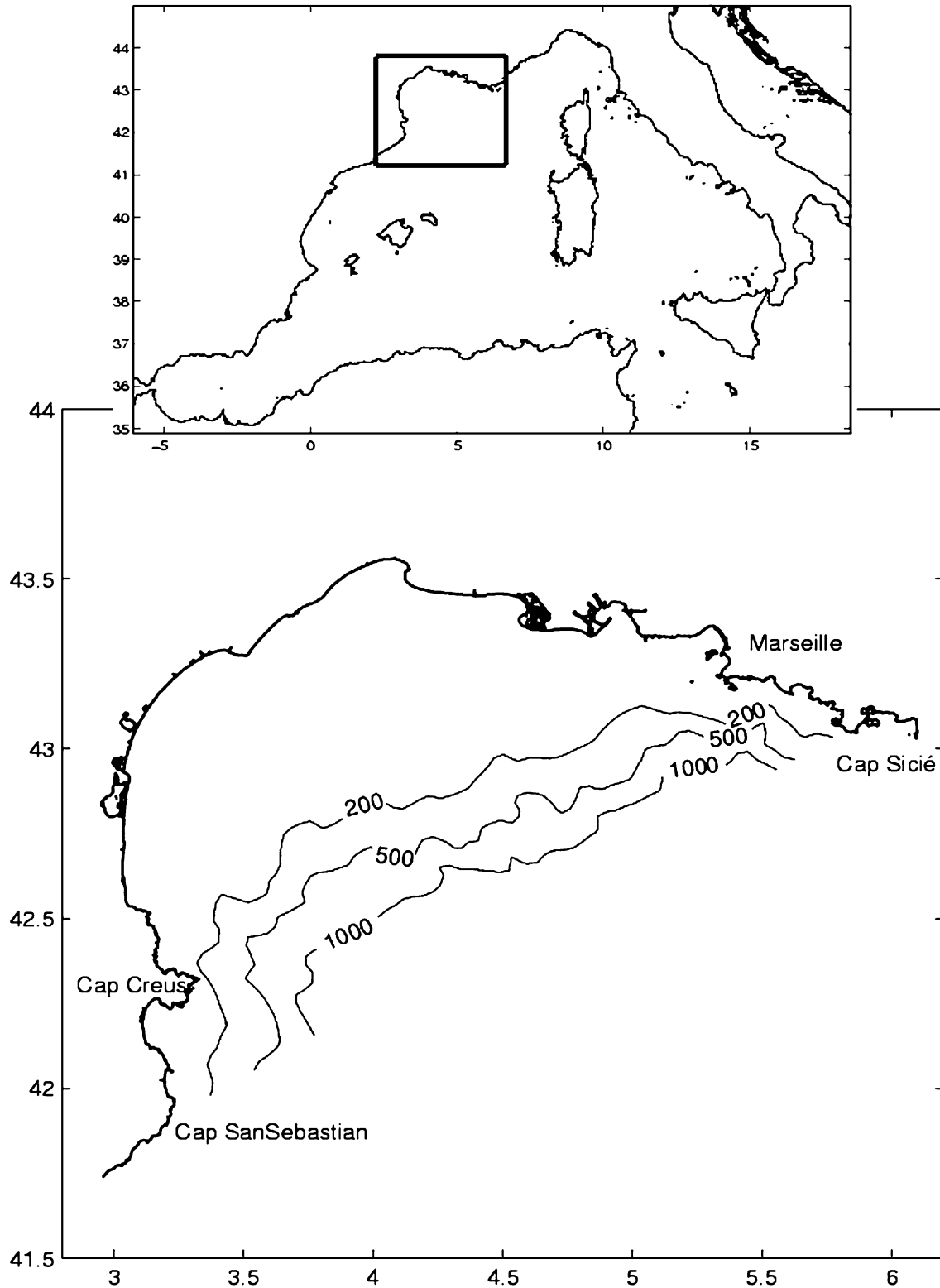


Fig. 1 Location of the Gulf of Lions inside the occidental Mediterranean Sea (*top*), and its bottom topography (*bottom*)

has been the subject of several works. The well-posed variational inverse problem in the elliptic formulation has been set up by Devenon (1990) for a tidal model of

the Seine bay. The ill-posed nature of the open boundary conditions in a shallow-water model was shown by Bennett and Chua (1994), but this can be solved by formulating the inverse problem as in Bogden et al. (1996) for the Massachusetts Bay. Moreover, the time dependency of the open-boundary conditions is well

adapted to variational analysis, which considers the space and time evolutions of the system as a whole. Such an approach has been applied in quasigeostrophic models of regional basins (Seiler 1993; Gunson and Malanotte-Rizzoli 1996). Continuing on these latter works, a data-assimilation method based on the rigid-lid OPA primitive-equation model is developed in order to estimate the initial and time-dependent open-boundary conditions relative to a remote influence.

Variational methods for initial and open-boundary conditions can support a space–time monitoring of a coastal basin by refining large-scale forcing fields to coastal scales. Apart from the operational point of view, sensitivity studies can in hindcast mode can evaluate the performance of an observational network design. This is the aim of the present article for the surface current measurements displayed in the Gulf of Lions area. In its first step, the data-assimilation system is applied in the academic configuration of a non-stratified flat-bottom open basin to detect a perturbation in the barotropic external forcing. The article is organized as follows: Section 2 contains a brief description of the inverse modelling system. Section 3 contains a description of the twin experiments run over the Gulf of Lions. Results are analyzed in Section 4 and discussed in Section 5. A conclusion is drawn in Section 6.

2 Methods

2.1 Data-assimilation system

Let us consider the forward problem which searches the circulation \mathbf{u} inside the open domain during the time window $[t_o, t_n]$, given the model parameters \mathbf{x} . This problem can be formally expressed by the relation:

$$\mathbf{u} = M_{NL}(\mathbf{X}) \quad (1)$$

where the non-linear model M_{NL} solves the primitive equations which describe the hydrodynamics (developed in next section). The solution \mathbf{u} represents the four-dimensional interior velocity field during the period (t_o, t_n) . For the present application, this model state is completely defined by model parameters composed of the initial condition \mathbf{x}_i and the time-dependent open-boundary condition \mathbf{x}_{ob} . The corresponding inverse problem searches an estimation of $\mathbf{x} = (\mathbf{x}_i, \mathbf{x}_{ob})$ from interior observations \mathbf{y}^{obs} taken during (t_o, t_n) . The estimation of these so-called control parameters is performed by minimizing the least-squares misfit between model state and observations according to the optimal control theory (Lions 1968), i.e. find $\mathbf{x}^{opt} = \min J(\mathbf{x})$ with

$$J(\mathbf{x}) = 1/2 \|\mathbf{y}^{obs} - \mathbf{y}\|^2 + 1/2\alpha (\|\partial_{ob}\mathbf{X}_{ob}\|_x^2 + \|\partial_t\mathbf{X}_{ob}\|_x^2) , \quad (2)$$

where $\mathbf{y} = H\mathbf{u}$, H being the linear projection of the model state onto the set of observations. Two terms penalizing the space (∂_{ob}) and time (∂_t) first derivatives

of \mathbf{x}_{ob} as a type of a priori information are added to the model-data misfit J_{obs} (Menke 1984). This regularization term J_{reg} is weighted by a non-dimensional positive coefficient α whose value has to be tuned, as discussed in Section 4. Then, the cost function can be written $J = J_{obs} + \alpha J_{reg}$. In the same way, the error associated with each observation is inserted in the norm $\|\cdot\|$, defined by the inner product $\langle y_1, y_2 \rangle = y_1^T R^{-1} y_2$, where R is a diagonal matrix of error variances.

The minimum search is reduced to a set of control parameters consistent with the physics and close to the prior estimate of the controls at the beginning of the optimization. The descent-direction algorithm M1QN3 (Gilbert and Lemaréchal 1989), a quasi-Newtonian method, is used. It obtains the input information of the cost function J and its gradient according to the control parameters $\nabla_x J$ to direct them toward the optimal control \mathbf{x}^{opt} :

$$\mathbf{x}_{k+1} = \mathbf{x}_k - \Gamma \cdot \nabla_x J , \quad (3)$$

where the step operator Γ is evaluated by approximations of the inverse Hessian of J , given the large dimension of the problem ($\sim 10^5$). Because the cost function is an implicit function of \mathbf{x} , its gradient is calculated with the adjoint code (Le Dimet and Talagrand 1986; Talagrand and Courtier 1987). The model M_{NL} solving the forward problem (Eq. 1) is differentiated according to the control parameters around \mathbf{x}_0 to obtain the corresponding tangent linear model $M(\mathbf{x}_0)$.

$$\delta \mathbf{u} = M_{NL}(\mathbf{x}_0 + \delta \mathbf{x}) - M_{NL}(\mathbf{x}_0) \approx M(\mathbf{x}_0) \cdot \delta \mathbf{x} . \quad (4)$$

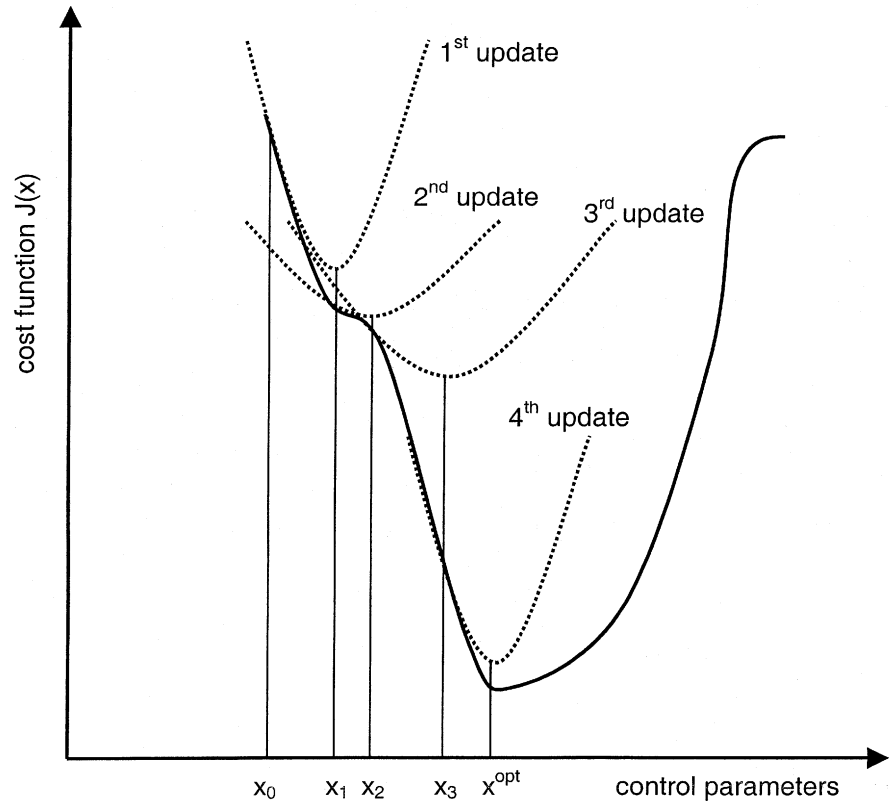
The adjoint model of $M(\mathbf{x}_0)$ and noted $M^*(\mathbf{x}_0)$ is forced by the model-data misfit to attain the gradient $\nabla_x J$:

$$\nabla_x J = M^*(\mathbf{x}_0) \cdot H^T \cdot (\mathbf{y} - \mathbf{y}^{obs}) \quad (5)$$

This brief description of the adjoint formulation is identical to that given by the Lagrange multipliers in the discrete case. In this four-dimensional approach, all the observations, collected at different times, are used to find the optimal control \mathbf{x}^{opt} .

The implementation of this data-assimilation method is based on the adjoint of the OPA model dedicated to initial condition control in the Equatorial Pacific Ocean (Weaver et al. 2003). An incremental formulation is used. It consists in periodic updates of the innovation vector $(\mathbf{y}^{obs} - \mathbf{y})$ with the forward model M_{NL} ; in between each update, the minimization of a quadratic cost function around a prior trajectory is performed in a loop involving $M(\mathbf{x}_0)$ and its adjoint $M^*(\mathbf{x}_0)$. The sequence of locally optimal controls converges to the minimum of J (Courtier et al. 1994), as shown in Fig. 2. For application to the open-boundary control, the tangent and adjoint codes have been adapted according to these additional parameters. The time series \mathbf{x}_{ob} is then projected at the time step t in (t_o, t_n) to a value $\mathbf{x}_{ob}(t)$ taking all the model dynamical constraints into account (see Sect. 2.3 and Appendix). The set of projectors and their corresponding adjoint operators are implemented as explicit rules in the tangent linear and adjoint codes, to

Fig. 2 Scheme of the 4DVAR algorithm in its incremental configuration. The series of control parameters from the prior estimate x_0 to the optimal control x^{opt} is performed after several updates of quadratic minimization problems



become exact constraints for the minimization problem instead of variational ones if included in cost function.

2.2 Forward model M_{NL}

The model solves the primitive equations in rigid lid approximation. The version used for the assimilation algorithm involves basic physics, given in detail in Madec et al. (1998), and applied hereafter to a non-stratified basin. The homogeneous water motions are described by a momentum balance Eq and a continuity equation:

$$\partial_t \mathbf{u} + (\mathbf{u} \cdot \nabla) \mathbf{u} + w \partial_z \mathbf{u} + f \mathbf{k} \wedge \mathbf{u} = -1/\rho_0 \nabla p + \nu_1 \nabla^4 \mathbf{u} + \nu_v \partial_{zz}^2 \mathbf{u} \quad (6)$$

$$\nabla \cdot \mathbf{u} + \partial_z w = 0, \quad (7)$$

where \mathbf{u} is the horizontal velocity, w is the vertical velocity, p is the surface pressure given a zero hydrostatic pressure gradient, ∇ is the horizontal gradient, ρ_0 is the constant density of the fluid, f is the Coriolis factor and \mathbf{k} is the upward unit vector. The turbulence closure is parameterized by constant viscosity coefficients ν_1 and ν_v . In the rigid lid approximation, the barotropic transport \mathbf{U} is non-divergent owing to the vertical integration of Eq. (7). Then it can be derived from a stream function ψ :

$$\mathbf{U} = \mathbf{k} \wedge \nabla \psi. \quad (8)$$

This assumption allows the surface pressure gradient to be diagnosed. The vertical integration of the momentum

balance from the bottom at the depth h to the surface leads to:

$$1/\rho_0 \nabla p = 1/h \mathbf{m} - 1/h \mathbf{k} \wedge \nabla \partial_k \psi. \quad (9)$$

Here \mathbf{m} represents the depth-integrated collected contributions of forcing terms and dissipation terms in the momentum balance Eq (2.6):

$$\mathbf{m} = 1/\rho_0 (\boldsymbol{\tau}_s - \boldsymbol{\tau}_b) + \nu_1 \nabla^4 \mathbf{U} - f \mathbf{k} \wedge \mathbf{U} - \int_{[0,h]} [(\mathbf{u} \cdot \nabla) \mathbf{u} + w \partial_z \mathbf{u}], \quad (10)$$

where $\boldsymbol{\tau}_s$ (or $\boldsymbol{\tau}_b$) represents the surface (or bottom) friction. The curl of the surface pressure gradient (Eq. 10) leads to an elliptic equation verified by the stream function trend:

$$\nabla \cdot (1/h \nabla \partial_t \psi) = \mathbf{k} \cdot (\nabla \wedge 1/h \mathbf{m}). \quad (11)$$

Thus, the surface forcing (included in \mathbf{m} , Eq. 10) acts on the barotropic flow through its spatial variations as expressed by the relation (11). These variations are directly related to the surface depressions (∇p , relation 9). More precisely, the surface pressure gradient is the predominant forcing term in the momentum balance. It is directly related to the sea-surface slope in free surface modelling. The present model filters out all surface gravity waves. Coastal dynamics represented by the model equations are restricted to long time scale motions compared to the inertial period. Moreover, perturbations of characteristic length lower than the radius of deformation are instantaneously adjusted.

Considering the case of cross-shore wind setup in a non-rotating basin, the equilibrium between the surface pressure gradient (not equal to zero although the horizontal sea surface) and the wind stress occurs instantaneously (Eq. 9) as the transport is zero (Eq. 11). All transient motions due to gravity waves that occur during adjustment of the free surface are not represented because considered as high-frequency signals by the model.

In the present study, M_{NL} computes the time evolution of the wind-induced slow-varying motions given by the horizontal velocity field. The time evolution of tracers is not computed in this non-stratified case. The coastal bay is limited by a continuous coastline and by a straight open boundary offshore, where the large-scale circulation is prescribed. The influence of the offshore circulation is introduced by the specification of the whole time series of the current profile along the open boundary. A free-slip condition for the current is chosen along the coastline. A leapfrog numerical scheme with a time step of 30 min is used on an isotropic C grid of horizontal resolution equal to 3.7 km. The vertical discretization from 0 to 500 m depth uses 16 z levels, with 8 levels in the top 60 m. The kinetic energy is partly dissipated by a bottom friction τ_b proportional to the current. The corresponding decay time is ~ 100 days. Energy is diffused by the lateral biharmonic diffusion scheme, using a constant value set to $\nu_1 = 10^9 \text{ m}^4 \text{ s}^{-1}$. For the open-boundary treatment, the diffusion scheme is harmonic. The vertical diffusion uses an implicit scheme with a constant $\nu_v = 10^{-1} \text{ m}^2 \text{ s}^{-1}$. Hence, the vertical structure of the current is given by a surface Ekman layer of ~ 50 m depth at the mid-latitude situation of the basin ($f = 10^{-4} \text{ s}^{-1}$). Finally, each time iteration requires the resolution of a non-homogenous elliptic problem given by Eq. (11) and a Dirichlet condition to be specified on lateral boundaries. This condition is actually zero at the coastline. Otherwise, it is expressed by a spatial integration of the transport trend $\int_{AM} \partial_t \mathbf{U} \cdot d\mathbf{M}$ from the west border point A to a travelling point M along the open boundary.

2.3 Set-up of a twin experiment

The present study focuses on the barotropic influence of the large-scale circulation. Therefore, the data-assimilation method described in Section 2.1 is set up to control only the sensitive model parameters which are related to the transport field. For the sake of preserving a computational homogeneity, a transport trend condition ($\partial_t \mathbf{U}$) is specified and controlled at the open boundary as the velocity trend ($\partial_t \mathbf{u}$) and the stream function trend ($\partial_t \psi$) are computed at each time step. In consequence, the control parameters are composed of the initial transport field $\mathbf{x}_i = \mathbf{U}(t_o)$; the along-boundary component of $\partial_t \mathbf{U}$ and noted $\mathbf{x}_{\text{tob}}[t \in (t_o, t_n)]$; the cross-boundary component of $\partial_t \mathbf{U}$ and noted $\mathbf{x}_{\text{nob}}[t \in (t_o, t_n)]$. Details for the evaluation of the gradient $\nabla_x \mathbf{J}$ according

to these specific control parameters are given in the Appendix.

The data-assimilation system is applied to a twin experiment. A model run which starts from perturbed controls generates a synthetic dataset. The goal of the twin experiment is to find again these perturbed control parameters by assimilating the model-generated observations. When such an identical test case is validated, the quality of the perturbed control estimation is a function of the quality of the dataset assimilated. The twin experiment is able to validate improvements in the observational network. The optimization procedure is set up to a series of outer loops (which update the reference trajectory in the incremental approximation) composed of three inner loops (which solve the local quadratic optimization problems, see Fig. 2). A measure for the speed of this procedure is given by the number of calls to M1QN3 (hereafter the number of simulations). Attention is paid to the preconditioning of \mathbf{x} in the case of the two components of initial conditions (dimension of a transport) and open-boundary conditions (dimension of a transport trend). At this point, two global reduction rates are defined. Their value inside the interval (0,1) increases with the optimization efficiency:

$$\sigma_u = 1 - \|\mathbf{u}^{\text{obs}} - \mathbf{u}^{\text{opt}}\| / \|\mathbf{u}^{\text{obs}} - \mathbf{u}^{\text{bck}}\| . \quad (12)$$

σ_u measures the adjustment of the optimized model state to the observed.

$$\sigma_x = 1 - \|\mathbf{x}^{\text{obs}} - \mathbf{x}^{\text{opt}}\|_x / \|\mathbf{x}^{\text{obs}} - \mathbf{x}^{\text{bck}}\|_x . \quad (13)$$

σ_x measures the adjustment of the optimal control to the perturbed control. This rate can be reduced to the across (resp. along) open boundary conditions adjustment $\sigma_{x_{\text{nob}}}$ resp. $\sigma_{x_{\text{tob}}}$ adjustment and to the initial condition adjustment σ_{x_i} . Notice that these rates are equal to zero at the start of the optimization. The computation of a twin experiment requires full storage of the model state \mathbf{u} ; hence, the following numerical experiments have been performed on an NEC-SX5 supercomputer.

3 Experiments

3.1 Academic configuration and dynamics

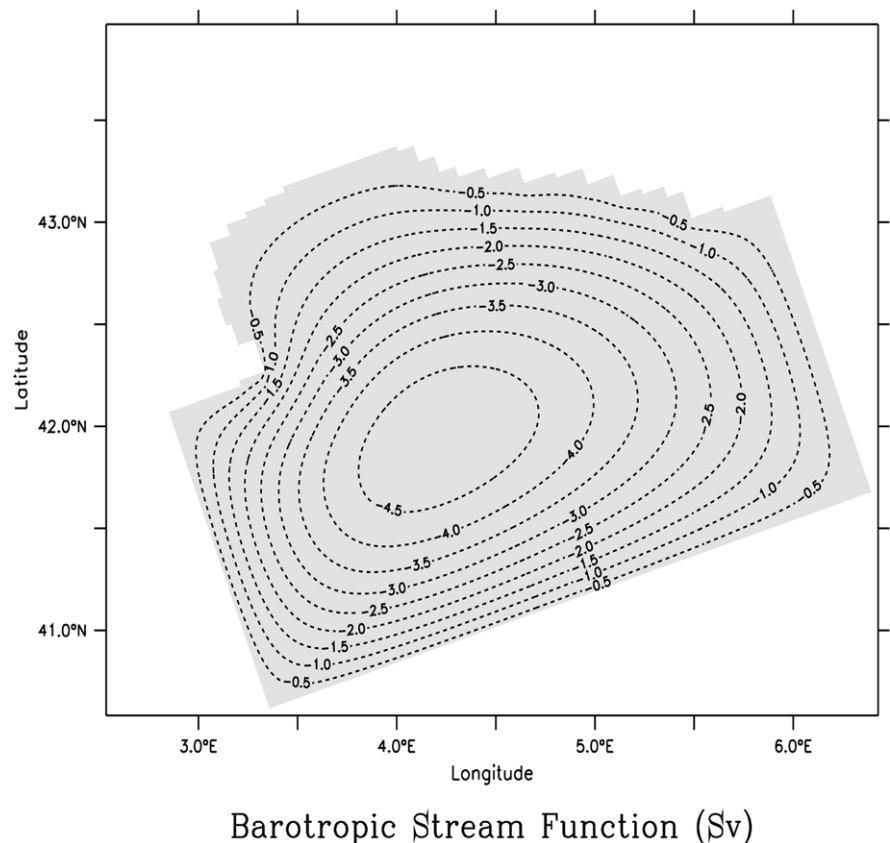
Let us consider the northwestern Mediterranean Sea from Cap Sicié to Cap San Sebastian that includes the Gulf of Lions shelf and its bending slope (Fig. 1). The area is 300 km long and 110 km wide. The circulation over the Gulf of Lions is influenced by the spatial and temporal variations of the Liguro-Provençal Current, which flows along the slope bending the shelf (Millot, 1990; Auclair et al. 2001). The nature of this interaction has been explored by analytical studies (Echevin et al. 2003) based on a two-layer model. Events of intrusion of this large-scale current are shown to have a barotropic component that affects the whole shelf due to a corresponding radius of deformation larger than the basin extensions.

Model configuration and dynamics are chosen to represent in a basic way the large-scale and low-frequency barotropic adjustment of the coastal bay circulation to an offshore perturbation. The open basin geometry is actually simplified to a flat bottom and a rough coastline. The circulation pattern is composed of a large-scale current flowing from east to west through the bay. A basin model that includes a coastal bay is used to provide consistent open boundary current. Its spatial resolution and physical parameterizations are identical to those of the coastal model. For the sake of simplicity, the effect of topography (mainly due the slope bending the Gulf of Lions shelf) is removed: the whole basin has a flat bottom of 500 m depth. It extends over an area 350 km long and 300 km wide. A large basin-scale cyclonic gyre is generated by an imposed constant positive wind-stress curl. The northern branch of the gyre can be considered similar to the Liguro-Provençal Current (Herbaut et al. 1997). The basin-scale circulation in steady state is represented in Fig. 3. A perturbation of the wind-stress curl is imposed out of the bay region and generates an adjustment over the whole basin by the propagation of a barotropic Rossby wave. Because of the large radius of deformation (~ 700 km) and the dimensions of the basin, the adjustment is instantaneous. The cyclonic gyre intensity decreases, and hence the inflow to the coastal bay. The barotropic perturbation can be represented by the value and variations of this incoming flow.

3.2 Sensitivity study

Given the nature and the spatial scale of such an adjustment, our goal consists in the design of efficient space-time monitoring networks for the detection of the barotropic signal of the intrusion. High-frequency signals play a small part in the Gulf of Lions circulation in winter during gusts of northern wind (mistral) because of its poor stratification and tide (Estournel et al. 2003). Thus, observations during this period are mainly representative of low-frequency barotropic signals. Three different datasets composed of surface current observations are involved over the bay. The first set (called TRANS) involves a full-time measurement taken at each time step along the two transects T1 and T2 (shown in Fig. 4a). The line T1 closing the bay is the farthest crossing taken by coastal surveys covering the Gulf of Lions. Four time series taken at the mooring points M1 to M4 along the transect T1 are extracted from the TRANS dataset (see Fig. 4b). The second dataset (called MOOR) keeps two values per day of these four time series. The associated observational error covariances take into account the weighted contribution of the closest grid points to obtain a larger spatial insight. The third dataset called SARHY, is composed of measurements at a travelling point with a speed of 7.5 knots along transects shown in Fig. 4c. This set simulates the databases of SARHYGOL surveys (Petrenko 2003) taken in a non-stratified winter situation of the Gulf of

Fig. 3 Steady-state barotropic circulation (in Sv) in the basin model in which the coastal model is embedded



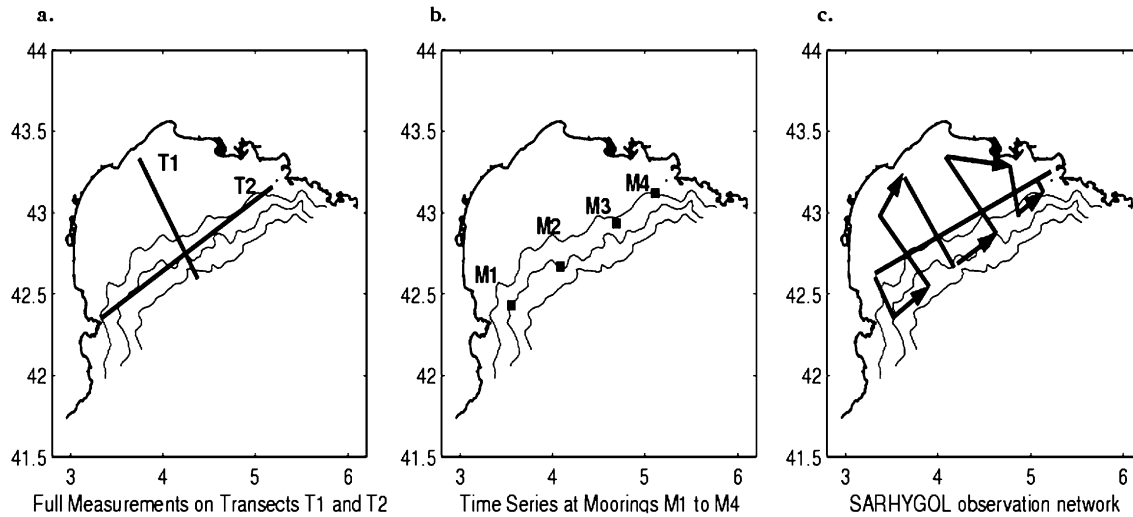


Fig. 4a–c The three networks of the gulf observation. **a** Full space and time measurements of the surface current along the transects T1 and T2 (TRANS). **b** Time series of the surface current at four mooring points M1 to M4 (MOOR). **c** Surface current measured at a travelling point along the SARHYGOL network with a speed of 7.5 knots (SARHY)

Lions. In practice, one observation of current is assimilated at each time step, and the SARHY network is travelled twice during the assimilation period. The observational errors are assumed to be independent (i.e. not correlated) with a homogeneous variance fixed to $(1 \text{ ms}^{-1})^2$.

Initial state (at the time t_0) and open-boundary velocity profiles [during the period $[t_0, t_n]$] for the coastal model are extracted from the basin model output. The assimilation period is set to 10 days. Without the perturbed open-boundary fields, the coastal model generates a steady circulation \mathbf{u}^{bck} and the prior estimate of control parameters \mathbf{x}^{bck} . The perturbed control parameters \mathbf{x}^{obs} and the corresponding observed coastal circulation \mathbf{u}^{obs} are provided by the basin model perturbed run. Synthetic data \mathbf{y}^{obs} are extracted from \mathbf{u}^{obs} and assimilated to estimate boundary controls. Two cases are studied: if the perturbation and its adjustment occur after t_0 , \mathbf{u}^{obs} is not influenced by initial conditions. Hence, only open-boundary conditions are controlled. If the perturbation occurs before t_0 , the initial conditions $\mathbf{u}^{\text{obs}}(t_0)$ are different from the prior estimate of the initial conditions $\mathbf{u}^{\text{bck}}(t_0)$. In that case, it is necessary to control both initial and open-boundary conditions.

4 Results

Four kinds of twin experiments are run on the basis of the latter academic configuration. First, the validity and performance of the open-boundary control is studied. Then the efficiency of the three observational networks to detect barotropic external perturbations is evaluated. The regularization term inserted in the cost function J (Eq. 2) is shut off in the case of perfect datasets: $\alpha = 0$ in

experiments A and B. Characteristics and results are presented below.

4.1 Experiments A

Let us consider the identification of the perturbed control parameters with the assimilation of the TRANS dataset. The optimization algorithm is validated only in the case of the control of open-boundary conditions (exp. A1) and in the case of the control of both initial and open-boundary conditions (exp. A2). Figure 5 shows the decrease of cost functions in exps. A1 and A2. Even if the minimum value (equal to zero) is not attained, most of the minimization is performed in the first 17 simulations with a reduction of 3 orders of magnitude. In comparison to exp. A1, there is a lesser decrease of the cost function in exp. A2. The analysis of the global reduction rates defined in Eqs. (12) and (13) and summarized in Table 1 leads to the same results. The adjustments to the observed state and the corresponding controls are mainly reached in the early minimization: the identification seems to be achieved in both experiments. Secondly, the quality of the minimization is less in the case of the estimation of both initial and open-boundary conditions. Note that the initial conditions are not identified in exp. A2, but this relatively poor estimation has little influence on the global reduction value σ_x . Furthermore, the small value of σ_{xtob} shows a poor control of the tangential parameters in exp. A1; it appears even weaker in exp. A2.

4.2 Experiments B

In the case of a non-perturbed initial state, the efficiency of the method faced with sparse datasets is studied. Even if the observations are perfect (i.e. not polluted by noise), their number should be the major restrictive factor for our assimilation procedure. The characteristics of the three experiments B are summarized in

Fig. 5 Decreasing cost function in exp. A1 (dashed line) and exp A2 (straight line) as a function of the number of simulations

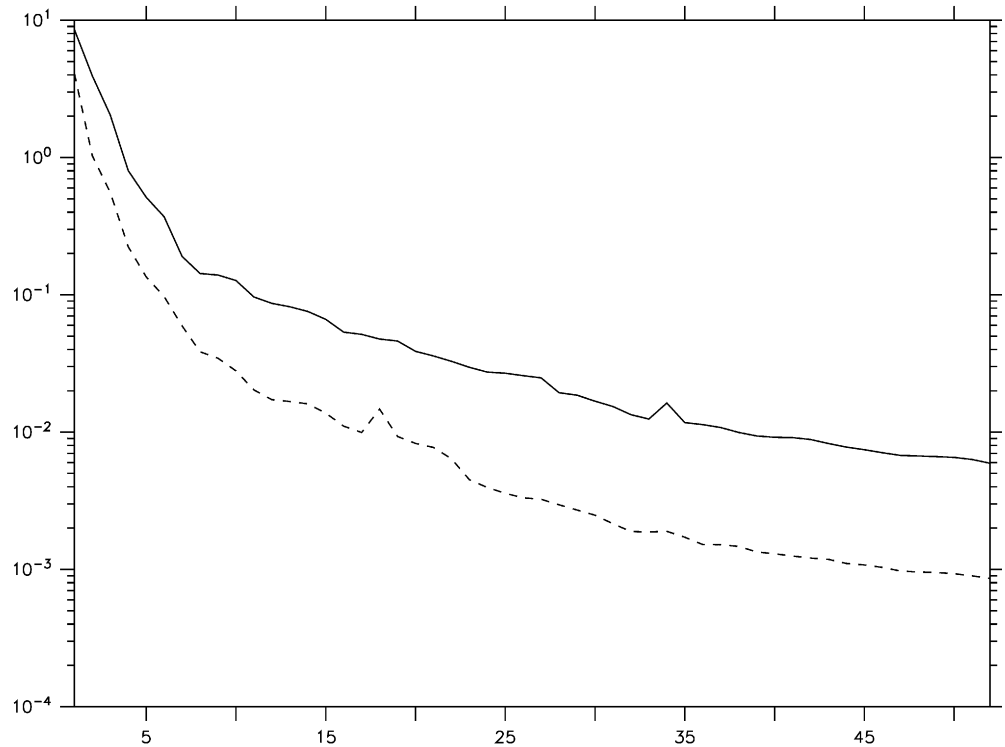


Table 2. A first estimate of the solutions is given after 17 iterations in the minimization for each experiment. The assimilation of the MOOR dataset is improved by the introduction of a time slope in the observational error variances. The data-model misfit is multiplied by a

Table 1 Experiments A involve the TRANS dataset (105 820 observations). The regularization term of the cost function is shut off ($\alpha = 0$). Global reduction rates defined in Eqs. (12) and (13) are measured after 52 simulations and 17 simulations

	exp. A1	exp. A2
Nature of controls	\mathbf{x}_{ob}	$\mathbf{x}_{ob}, \mathbf{x}_{ic}$
Number of controls	79 993	83 500
$\sigma_{\mathbf{u}}$	92.35%	90.00%
$\sigma_{\mathbf{x}_{nob}}$	96.20%	94.44%
$\sigma_{\mathbf{x}_i}$		66.74%
$\sigma_{\mathbf{x}_{tob}}$	44.32%	30.71%
$\sigma_{\mathbf{u}}$ after 17 simulations	87.47%	87.85%
$\sigma_{\mathbf{x}_{nob}}$ after 17 simulations	93.75%	93.03%

Table 2 Experiments B involve the estimation of \mathbf{x}_{ob} only from the MOOR and SARHY datasets without regularization ($\alpha = 0$). Global reduction rates are measured after 17 simulations

	exp. B1	exp. B2	exp. B3
Nature of data	MOOR	MOOR	SARHY
Obs error covariances	Constant	Time slope	Constant
Number of data	160	160	960
$\sigma_{\mathbf{u}}$	75.38%	79.89%	84.42%
$\sigma_{\mathbf{x}_{nob}}$	84.41%	89.33%	89.70%

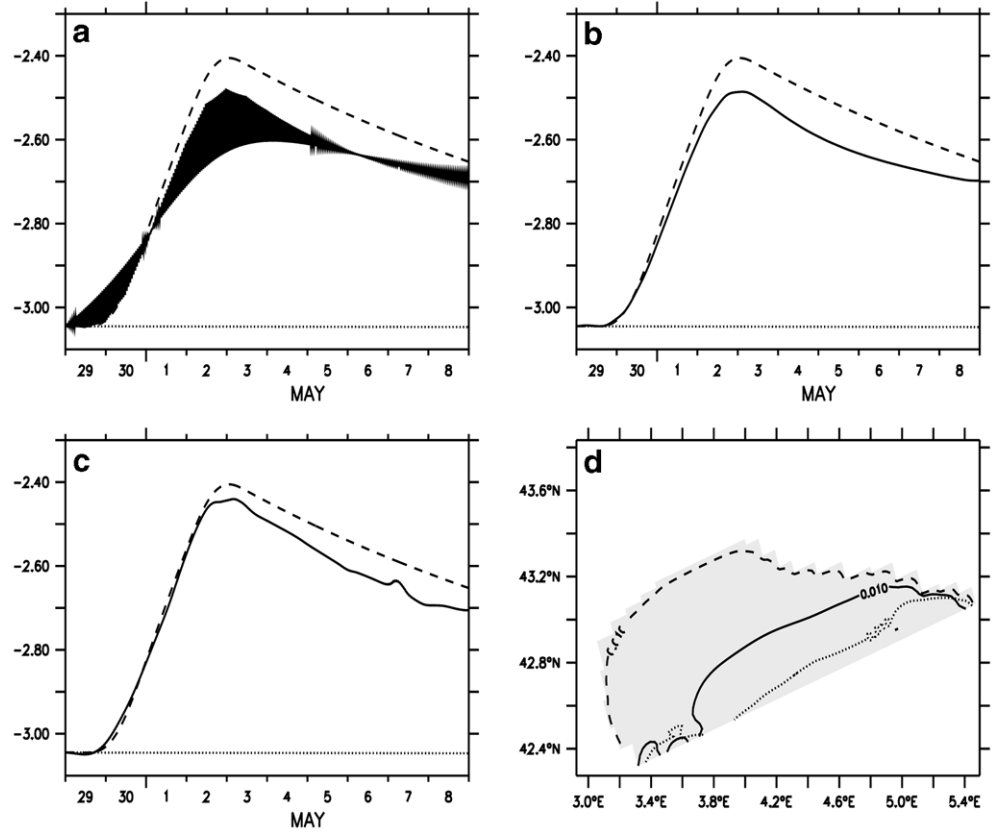
weighting factor that increases from 0 to 1, and back to 0, as the difference between the observation time and the model time goes from -6 h to $+6$ h. This time-weighting factor (Derber and Rosati 1989) allows a 12-h synoptic observation in the optimization procedure. The comparison between solutions from exp. B1 and exp. B2 shows the smoothing effect of this transformation. The highly unstable feature of the estimated incoming flow time series (Fig. 6a) is removed; the adjustments to the observed circulation and corresponding perturbed across open-boundary transport are improved (Fig. 6b).

Now, let us consider the assimilation of the two datasets MOOR and SARHY. As shown in Table 2, their size is on the same scale as the set of control parameters. An objective comparison of the solution sensitivity to these two datasets is considered in exps. B2 and B3. If the adjustment to the perturbed across-boundary transport is similar in the two experiments (see Fig. 6b, c), the optimal control in exp. B3 leads to a circulation closer to the observed. The global reduction rate to the observed model state is better than in exp. B2. Moreover, the spatial representation of the difference between the mean observed and estimated circulation (Fig. 6d) shows a smaller area of more than 0.01 Sv discrepancy for exp. B2, located along the open boundary.

4.3 Experiments C

In this section, the observations of the SARHY dataset are no longer considered perfect, and a Gaussian noise,

Fig. 6a–d Representation of the observed incoming flow into the bay (*dashed line*) and the optimized one (*straight line*) from exp. B1 (**a**), exp. B2 (**b**), exp. B3 (**c**); the prior estimate is represented by the *horizontal dotted line*. **d** Spatial representation of the isoline 0.01 Sv of the misfit between observed mean circulation and the optimized mean circulation, from exp. B2 (*straight line*) and exp. B3 (*dotted line*); the prior estimate misfit is in *dashed line*



whose mean is zero and whose amplitude increases from 5 to 20% of the signal, is added to the observations. The optimization procedure allows a robust estimation of the open-boundary conditions only in the case of a weak noise level. Optimized solutions from exps. C1 and C3 stay close to the observed solution, as shown in Table 3. The estimated solutions are improved by the introduction of the regularization term J_{reg} in the cost function (expressed in Eq. 2), as done in exps. C2, C4 and C5. Note that without any a priori knowledge of the control parameters, the classical penalization on the fit to the first guess would be useless in the present case: such a term would restore the solution to the steady state. The value of the non-dimensional parameter α cannot be fixed a priori. Hence, the determination of an optimal value for α was made a posteriori for each experiment. The assimilation procedure is run for exps. C2, C4 and C5, respectively, with different values for α . After nine simulations, the optimal value is the one that maximizes

both σ_u and σ_x , as shown in Fig. 7. We find an accentuation of the regularization weight as the noise level increases.

Agreement with the observed circulation is improved by the introduction of the regularization term (see Table 3). When the noise level increases from 5 to 10%, the improvement becomes more significant in both rates σ_u and $\sigma_{x_{\text{nob}}}$. The weight of J_{reg} increases when the noise level increases. In Fig. 8, the result on the analyzed incoming flow through the bay shows the time-smoothing effect of this constraint, which is amplified with increasing α values.

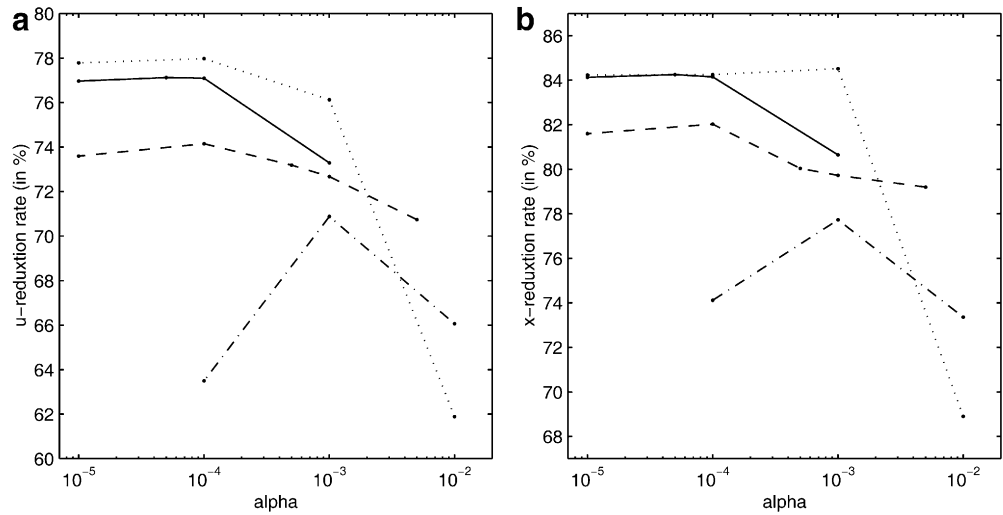
4.4 Experiments D

In this section, the control parameters are initial and open-boundary conditions. The SARHY dataset is used to estimate the initial and open-boundary conditions in

Table 3 Experiments C involve the estimation of x_{ob} from the SARHY dataset with different noise levels and regularization rates. Global reduction rates are measured after nine simulations

	exp. C1	exp. C2	exp. C3	exp. C4	exp. C5
Noise level	5%	5%	10%	10%	20%
α^{opt}	0	5×10^{-5}	0	10^{-4}	10^{-3}
σ_u	77.01%	77.12%	70.55%	74.15%	70.88%
$\sigma_{x_{\text{nob}}}$	84.53%	84.25%	80.09%	82.03%	77.73%

Fig. 7a, b Research of α^{opt} maximising the values σ_u (a) and $\sigma_{x_{nob}}$ (b) for exp. C2 (straight lines), exp. C4 (dashed lines), exp. C5 (dot-dash lines) and exp. D3 (dotted lines)



three experiments which involve different noise levels. Their characteristics and global performance are summarized in Table 4. Given the reduced number of simulations (compared to exp. A2), the adjustment to the

observed circulation is only obtained roughly, as the minimization is not yet achieved. A regularization term is introduced from a 10% noise level, with a weight determined a posteriori, as described previously. During the first iterations of the minimization, the adjustment to the initial conditions is improved as the noise level increases.

Figure 9 shows a comparison between the circulation obtained in exps. D1 and D3. The agreement to the observed initial circulation is systematically underestimated by 0.1 Sv in both experiments. The adjustment of the initial to the observed circulation (Fig. 9b) is more efficient in exp. D3 (Fig. 9d) than in exp. D1 (Fig. 9c). Notice the regularity in the spatial adjustment: there is no region inside the basin where the optimized circulation becomes improved compared to others. Instead, the time evolution of the analyzed incoming flow is better in exp. D1 (Fig. 9a), as the discrepancy at the initial time is quickly reduced in both experiments.

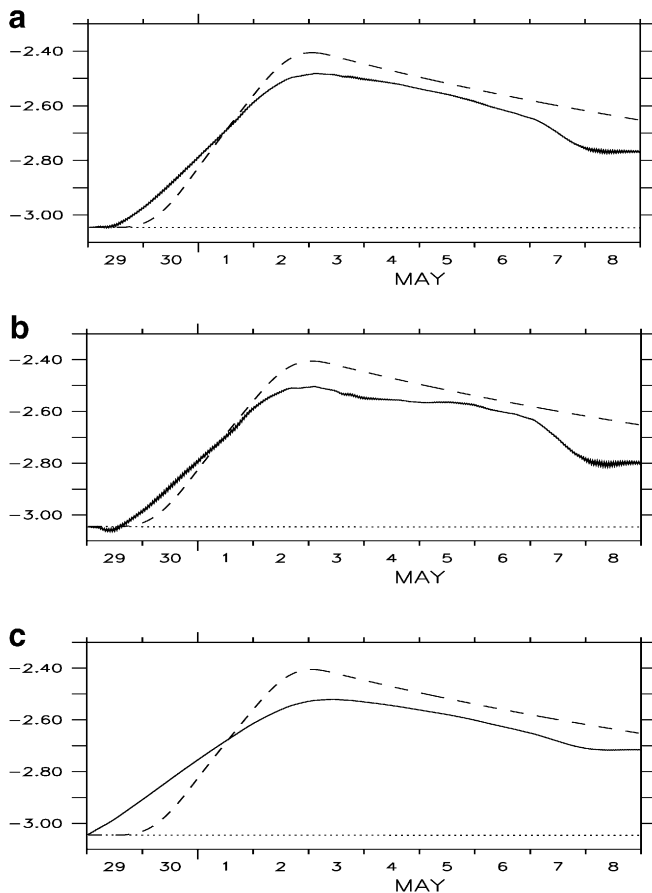


Fig. 8a-c Optimized gyre incoming flow (straight line) from SARHY dataset with three different noise levels: a exp. C2; b exp. C4; c exp. C5

5 Discussion

5.1 Identification of the control parameters

Experiments A involve overdetermined inverse problems, while the number of control parameters is lower than the number of observations. Because of this overdetermination, the theoretical minimum of the cost function J is zero. This theoretical minimum is not attained numerically, because the decrease of J after 17 iterations is weak. Moreover, the theoretical optimal control is unique and equal to the perturbed control. In the two experiments A1 and A2, the set of control parameters is mainly composed of open-boundary conditions. The across-boundary transport x_{nob} reaches its optimal value. Its contribution to the dynamics of the coastal bay through the surface

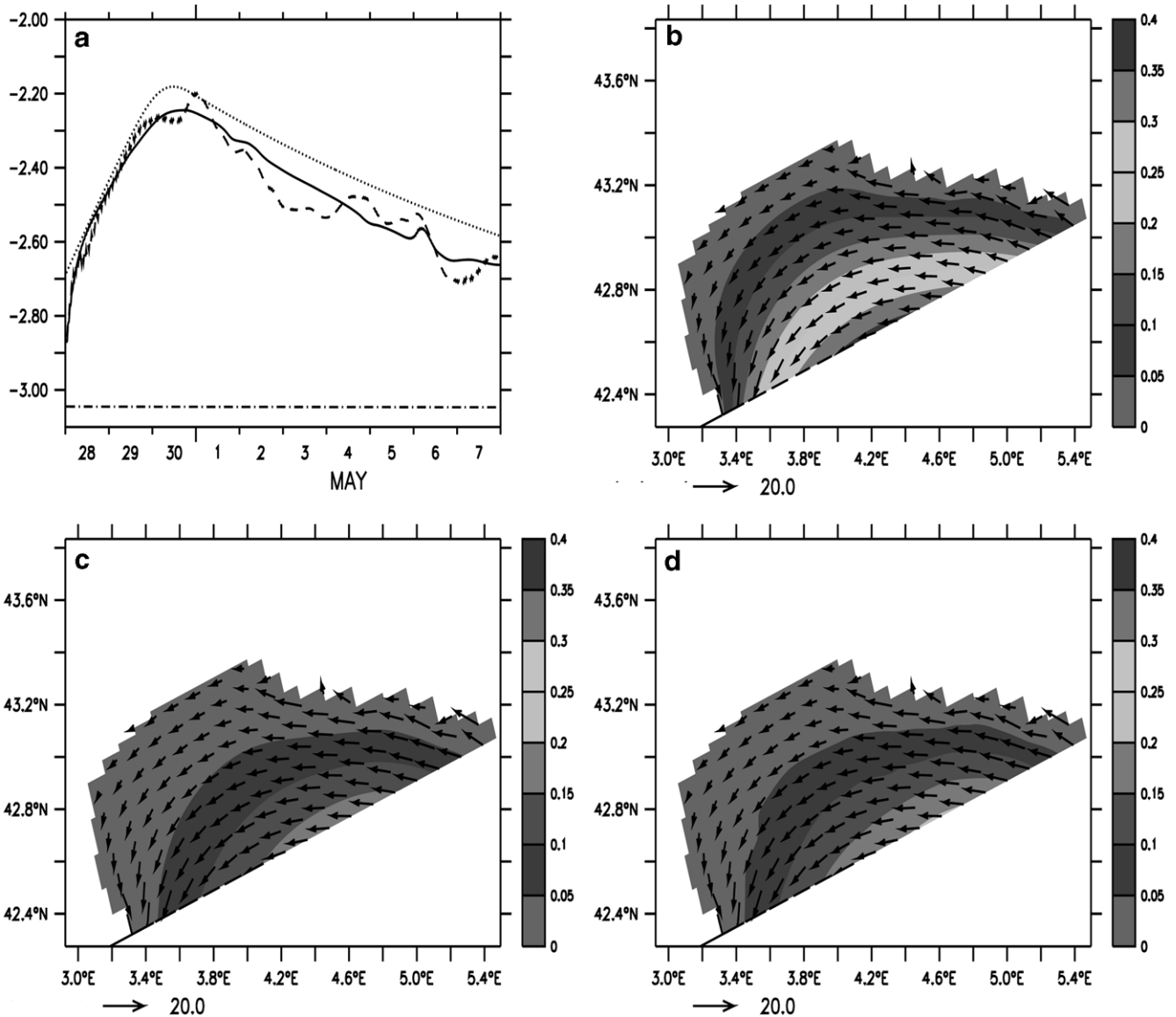
Table 4 Experiments D involve the estimation of x_i and x_{ob} from the SARHY dataset with different noise levels and regularization rates

	exp. D1	exp. D2	exp. D3
Noise level	0%	5%	10%
α^{opt}	0	0	10^{-4}
nb of simulations	25	17	25
σ_u	83.67%	80.00%	78.76%
$\sigma_{x_{nob}}$	88.04%	86.29%	84.89%
σ_{x_i}	44.60%	48.88%	54

Fig. 9 **a** Evolution of the incoming flow: the observed (*dotted line*), the prior estimate (*dash-dot line*), the solutions from exp. D1 (*straight line*) and exp. D3 (*dashed line*). Depth-averaged velocity field (in cm s^{-1}) and the discrepancy with the steady circulation (streamlines in Sv) at the initial time: the observed initial state (**b**), the optimized states from exp. D1 (**c**) and exp. D3 (**d**)

pressure gradient affects the whole bay circulation. Hence, it is the main control element of the experiments (in number and in contribution), and thus the best estimated control.

In contrast, the along-boundary current makes only a local contribution through dynamic processes involving velocity shear along the open boundary. Such processes are not very active in the present experiments. Even if the representation of the tangential velocities in the set of controls is equivalent to that of the normal velocities, the estimation of the former is masked by the normal component optimization. Tangential boundary parameters were kept only in the set of control parameters to produce optimized solutions of the barotropic current which are consistent with the coastal dynamics. The numerical noise due to conflicts between an optimized tangential current inside the basin and a fixed one along the open boundary is filtered automatically from the admissible solutions of the forward model. Concerning



the initial condition estimation in exp. A2, full identification is not reached. The initial parameters make a major contribution in the dynamics description. They have to be estimated to prohibit discontinuities between the optimized initial open-boundary conditions and the fixed initial field inside the domain; but their number inside the full set of controls is weak (30 times less), which could lower their representativity during the minimization.

In summary, these identification experiments show that normal transports are the major controls, whereas initial conditions and along boundary conditions are the weakest controls.

5.2 Sensitivity to the observational networks

We discuss in this section the solutions obtained along the open boundary by assimilating the TRANS (exps. A1, A2), MOOR (exps. B1, B2) and SARHY (exps. B3, D1) perfect datasets. At first, the number of assimilated observations leads to a different position for the inverse problem. If exp. A is overdetermined, MOOR and SARHY data-assimilation problems are posed in highly under-determined systems. Hence, the optimal control is not unique: there are theoretically, infinite solutions. In all the experiments, the results show a correct global adjustment to the observed incoming flow: more than 85% of the perturbation is estimated after 17 simulations. In exp. A, the massive data are used to accentuate the convergence of the cost function toward the optimal. In the other experiments, the analysis algorithm uses the observation as well as possible to provide an optimal solution: the coupling between space-time propagation inserted in the momentum equations and the observed information are treated simultaneously in this 4DVAR method. Consequently, a sparse dataset is able to provide good open-boundary conditions if its distribution in the space-time domain is efficient.

This is particularly the case in experiments B. The time distribution of the data information seems to be crucial for the algorithm stability. It can be explained by the fact that the offshore perturbation is inserted in the model by a Dirichlet condition of an elliptic equation (Eq. 11, developed in Sect. 2.2). Hence, the propagation scheme uses at each time step a solution of this elliptic equation. The adjoint model forced by the data-model misfit (Eq. 5), developed in Sect. 2.1) is influenced by the time-independent resolution of the adjoint elliptic equation. Thus the stability of the propagation scheme requires the inverse problem to be forced at each time step. This is solved by the introduction of a “slope” in the construction of observational error correlations (exp. B2).

The influence of the spatial distribution of observations is studied in the comparison of a fixed network (MOOR) and of a travelling network on a ship (SARHY). The results given in the latter section show that a synoptic description of the coastal circulation with SARHY is more efficient. The assimilation of such a

time-distributed dataset is very suitable with a 4DVAR method. All the observations are used at once and not just before analysis, as in sequential assimilation methods. This allows a reduction of the dataset if the observational network is compatible with the description of the dynamics involved.

5.3 Robustness in the minimization in the case of noisy data

The 4DVAR algorithm works only under the assumption that the model is perfect. With the use of model-generated observations, errors can be added to the assimilated dataset. Thus, the method is evaluated in the case of noisy data under the single constraint of the model dynamics. Its robustness depends on the balance between the error level and the efficiency of this constraint. This is why we consider a series of short experiments C (only nine simulations) which involve increasing noise levels in the synthetic dataset SARHY. It is shown that the adjustment to the observed circulation decreases when errors increase beyond 10% of the observation value.

With the lack of a good prior estimate of the offshore perturbation, a regularization term for the control parameters J_{reg} is added to the cost function J . This term penalizes the roughness of \mathbf{x}_{ob} . Then, the inverse problem becomes over-determined with the constraint of minimum roughness in the control parameters. Whereas the quadraticity of J is increased to obtain a rough approximation of its minimum, the corresponding unique optimal control is not equal to the observed one due to the addition of noise. Moreover, the theoretical value for the minimum of J_{obs} is different from zero: it depends on the value of the weighting parameter α . Hence, an optimal balance between the weight of J_{obs} and J_{reg} needs to be determined by an estimation of the optimal value for α . The results show an increasing weight of the regularization term with an increasing observational error. J_{reg} is then necessary to obtain a robust solution, but the optimal control parameters diverge from the observed ones as its weight in the cost function increases.

5.4 Perturbation of the initial state

When considering a perturbation starting before the initial time of the assimilation period, the initial velocity field has to be estimated as well. Since the starting point of the \mathbf{x}_{ob} time series is defined by the initial open-boundary conditions (included in \mathbf{x}_i), the link between control parameters is resolved at the open boundary with intrinsic model constraints. In addition to the leapfrog propagation scheme, consistency is ensured by the assumption of the non-divergence of the barotropic flow checked at the initial time (see Appendix). This can explain the spatial regularity in the analysis of the initial state (as shown in Fig. 9). The results of the experiments

D show an improvement in the adjustment to the observed initial state when assimilating imperfect data with an increasing noise level. This is only a weak improvement because minimization is not achieved. Nevertheless, the convergence to perturbed initial controls is faster in such a case. Hence, the open-boundary conditions are more sensitive to imperfect observations than the initial conditions.

5.5 Toward a realistic situation of the Gulf of Lions

The assumption of a non-stratified model gives a good representation of the wintertime situation of the Gulf of Lions; but the large-scale forcing current (the Liguro-Provençal Current) flowing along the shelf slope in its steady regime has a baroclinic structure. Then, a stratified open-boundary profile and corresponding vertical velocity field have to be estimated to provide a realistic remote forcing through interactions with topography.

A realistic configuration of the Gulf of Lions should include its bending slope, surface forcing from climatology or from atmospheric model re-analyses, and the plume corresponding to the Rhône River. This needs incorporation of enhanced parameterisations for physical processes and estimation of additional model parameters, but the set of control parameters should depend on the characteristics of observations assimilated: its temporal and spatial scale have a major influence on the sensitivity of the control parameters. Furthermore, when large-scale basin models are used as a first guess, statistical analysis of the differences between the coastal and the basin models are necessary to infer the correct error covariances. Moreover, the variational data-assimilation method is given with a perfect model hypothesis. Even with elaborated physics instead of the present rough simplifications, the model errors will not be taken into account. That is why the addition of well-built data-model error correlations (given by the setup of the measuring instruments) and accurate prior estimates for the control parameters are necessary for realistic applications.

Finally, the Liguro Provençal Current, which may flow during episodes into the Gulf of Lions, has a speed of 1–2 Sv, depending on the season. The twin experiments involve an observed transport (~ 2.4 Sv) which is 20% less than the prior estimate (~ 3 Sv). Estimations of the observed transport magnitude are obtained with accuracy (less than 10%), which could encourage realistic applications with the required operational accuracy.

6 Conclusion

We have investigated the estimation of initial and lateral boundary conditions for a coastal model with a variational data-assimilation method. The methodology developed in the present article employs synthetic observations to be assimilated for the estimation of the

initial and time-dependent open-boundary currents which control the barotropic circulation. This method has been tested in a twin experiment which involves a barotropic perturbation coming from offshore. An accentuated sensitivity of the cross-boundary transport appeared among the set of control parameters. Furthermore, the space and time distributions of the observations influence the efficiency in the control of such time series. Synoptic data along ship crossings have actually a better impact on analyzed boundary conditions than data from a mooring network. Finally, the reliability of the method has been investigated in more difficult optimization tasks, using coarse datasets and introducing errors into the observations. This first investigation has succeeded in providing accurate external forcing fields consistent with model physics from time-varying observational networks. Following developments to stratified configurations can lead to realistic application in the Gulf of Lions area.

Appendix. Evaluation of $\nabla_x J$

We use a discretization in time of the forward operator and its variables. The model state at a time step t_k can be expressed as the product of intermediate forecast steps. We have the recurrence given by the time iteration:

$$\mathbf{u}(t_{k+1}) = M_{NL,k}(\mathbf{x})[\mathbf{u}(t_k)] \quad k = 0, \dots, n-1$$

as M_{NL} is decomposed in a series of time-stepping operators $M_{NL,k}$ each of them depending on the control parameters $\mathbf{x}(t_k)$. The initial control \mathbf{x}_i is constrained to belong to the set of non-divergent flows in the rigid lid assumption. Solutions from the optimization algorithm are then projected by the linear operator:

$$\Lambda^0 : \mathbf{x} = (\mathbf{x}_i, \mathbf{x}_{ob}) \rightarrow (1/h\mathbf{k} \wedge \nabla\Psi, \mathbf{0})$$

$$\text{with } \nabla \cdot (1/h\nabla\Psi) = \mathbf{k} \cdot \nabla \wedge \mathbf{x}_i.$$

The open-boundary control \mathbf{x}_{ob} is defined in practice in terms of a transport trend. Its cross-boundary component transport verifies a volume conservation property of the basin at each time. As the initial control vector, solutions from the optimization algorithm are projected on the set of conservative flows by the linear operator:

$$\Lambda_k : \mathbf{x} = (\mathbf{x}_i, \mathbf{x}_{ob}) \rightarrow [\mathbf{0}, \mathbf{x}_{ob}(t_k)]$$

$$\text{such as } \int_{ob} \mathbf{x}_{nob}(t_k) = 0, k = 0, \dots, n,$$

where \int_{ob} denotes the integration along the open boundary. In practice, the projection operators defined previously are coded as explicit rules in the tangent linear and adjoint models.

Let us consider the dataset $[\mathbf{y}^{obs}(t_k)]_{k=0,n}$. The cost function J is expressed by the whole contribution of the innovation vectors taken at each time step:

$$J = 1/2 \sum_{k=0,n} [\mathbf{y}^{obs}(t_k) - \mathbf{y}(t_k)]^T \cdot [\mathbf{y}^{obs}(t_k) - \mathbf{y}(t_k)] . \quad (A1)$$

A variation of \mathbf{J} in the direction $\partial \mathbf{x}$ is related to the time components of $\Delta_{\mathbf{x}} \mathbf{J}$ by:

$$\delta \mathbf{J} = \nabla_{(\mathbf{x}, 0)} \mathbf{J} \cdot \Lambda^0 \delta \mathbf{x} + \sum_{k=0, n} [\nabla_{[0, \mathbf{x} \text{ob}(t_k)]} \mathbf{J}] \cdot [\Lambda_k \cdot \delta \mathbf{x}] . \quad (\text{A2})$$

The differentiation of Eq. (A1) in the same direction $\delta \mathbf{x}$ gives:

$$\delta \mathbf{J} = \sum_{k=0, n} [\delta \mathbf{y}(t_k)]^T \cdot [\mathbf{y}^{\text{obs}}(t_k) - \mathbf{y}(t_k)] . \quad (\text{A3})$$

The model state increment around a fixed control point which appears in Eq. (A3) is propagated in the tangent linear model. Let us define the corresponding time stepping operators \mathbf{M}_k tangent of $\mathbf{M}_{\text{NL}, k}$. In the set of observations, the increment at the time t_p is defined in function of $\delta \mathbf{x}$:

$$\begin{aligned} \delta \mathbf{y}(t_p) = & \mathbf{H} \cdot \left[\prod_{j=p-1, 0} \mathbf{M}_j \right] \cdot [\Lambda^0 \cdot \delta \mathbf{x}] \\ & + \mathbf{H} \cdot \sum_{k=0, p-2} \left[\prod_{j=p-1, k+1} \mathbf{M}_j \right] \cdot [\Lambda_{k+1} \cdot \delta \mathbf{x}] \\ & + \mathbf{H} \cdot \Lambda_p \cdot \delta \mathbf{x} . \end{aligned} \quad (\text{A4})$$

The transposition of Eq. (A4) is inserted in Eq. (A3) to obtain an expression of the gradient of \mathbf{J} according to the initial conditions as a function of the innovation vector,

$$\nabla_{(\mathbf{x}, 0)} \mathbf{J} = \sum_{k=0, n} \left[\prod_{j=0, k-1} \mathbf{M}_j^T \right] \cdot \mathbf{H}^T \cdot [\mathbf{y}^{\text{obs}}(t_k) - \mathbf{y}(t_k)] \quad (\text{A5})$$

and the gradient of \mathbf{J} according to the element at time t_p of open boundary conditions series:

$$\begin{aligned} \nabla_{[0, \mathbf{x} \text{ob}(t_p)]} \mathbf{J} = & \mathbf{H}^T \cdot [\mathbf{y}^{\text{obs}}(t_{p+1}) - \mathbf{y}(t_{p+1})] \\ & + \sum_{k=p+2, n} \left[\prod_{j=p+1, k-1} \mathbf{M}_j^T \right] \\ & \cdot \mathbf{H}^T \cdot [\mathbf{y}^{\text{obs}}(t_k) - \mathbf{y}(t_k)] . \end{aligned} \quad (\text{A6})$$

We obtain a developed expression for the gradient which obeys the relationship (5) as a linear function of the innovation vector. The adjoint model acts as a product of transposed tangent linear successive operators which retropropagate the contribution of the data information. Note that the time location of this information affects the efficiency of the optimization procedure. If a single observation at time (t_0, t_n) is considered, information about the circulation at time θ should be taken into account in every initial control, but only in the open-boundary controls inside the time window $(t_0, \theta - 1)$.

References

Auclair F, Marsaleix P, Estournel C (2001) The penetration of the northern current over the Gulf of Lions (Mediterranean) as a downscaling problem. *Oceanolog Acta* 24: 529–544

- Beckers J-M, Brasseur P, Nihoul JCJ (1997) Circulation of the western Mediterranean: from the global to the regional scale. *Deep Sea Res* 44: 531–549
- Bennett AF, Chua BS (1994) Open-ocean modelling as an inverse problem: the primitive equations. *Monthly Weather Rev* 122: 1326–1336
- Blayo E, Debreu L (1999) Adaptive mesh refinement for finite difference ocean models: first experiments. *J Phys Oceanogr* 29: 1239–1336
- Bogden PS, Malanotte-Rizzoli P, Signell R (1996) Open-ocean boundary conditions from interior data: local and remote forcing of Massachusetts Bay. *J Geophys Res* 101: 6487–6500
- Chapman DC (1985) Numerical treatment of cross-shelf open boundaries in a barotropic coastal ocean model. *J Phys Oceanogr* 15: 1060–1075
- Courtier P, Thépaut J-N, Hollingworth A (1994) A strategy for operational implementation of 4D-Var, using an incremental approach. *Qua J Roy Meteorol Soc* 120: 1367–1387
- Csanady GT (1982) Circulation in the coastal ocean. *Environmental fluid mechanics*. Reidel, New York
- Derber J, Rosati A (1989) A global oceanic data assimilation system. *J Phys Oceanogr* 19: 1333–1347
- Devenon J-L (1990) Optimal control theory applied to an objective analysis of a tidal current mapping by HF radar. *J Atmosph Ocean Technol* 7: 269–284
- Echevin V, Crépon M, Mortier L (2001) Analysis of the mesoscale circulation in the northwestern Mediterranean Sea simulated in the framework of the Mediterranean Forecast System Pilot Project. *Annal Geophys* 21: 281–287
- Echevin V, Crépon M, Mortier L (2003) Interaction of a coastal current with a shelf topography, application to the Gulf of Lions shelf. *J Phys Oceanogr* 33: 188–206
- Estournel C, Durrieu de Madron X, Marsaleix P, Auclair F, Julliand C, Vehil R (2003) Observations and modelisation of the winter coastal oceanic circulation in the Gulf of Lions under wind conditions influenced by the continental orography (FETCH experiment). *J Geophys Res* 108: 8059, doi:10.1029/2001JC000825
- Gilbert JCh, Lemaréchal C (1989) Some numerical experiments with variable-storage quasi-Newton algorithms. *Math Program* 45: 405–435
- Gunson JR, Malanotte-Rizzoli P (1996) Assimilation studies of open-ocean flows, part 1. Estimation of initial and boundary conditions. *J Geophys Res* 101: 28457–28472
- Herbaut C, Martel F, Crépon M (1997) A sensitivity study of the general circulation of the western Mediterranean Sea, part 2. The response to atmospheric forcing. *J Phys Oceanogr* 27: 2126–2145
- Jones JE, Davies AM (1998) Storm surge computations for the Irish Sea using a three-dimensional numerical model including wave-current interaction. *Continental Shelf Res* 18: 201–251
- Le Dimet F-X, Talagrand O (1986) Variational algorithms for analysis and assimilation of meteorological observations: theoretical aspects. *Tellus* 38(A): 97–110
- Lellouche J-M, Devenon J-L, Dekeyser I (1998) Data assimilation by optimal control method in a 3D coastal oceanic model: the problem of discretization. *J Atmosph Ocean Technol* 15: 470–481
- Lions J-L (1968) *Contrôle optimal de systèmes gouvernés par des équations aux dérivées partielles*. Editions Dunod, France
- Madec G, Delecluse P, Imbard M, Levy C (1998) OPA 8.1, ocean general circulation model reference manual. LODyC/IPSL technical report 11, Paris, France, 91 pp (Available online at <http://www.lodyc.jussieu.fr/opa/>)
- Menke W (1984) *Geophysical data analysis: discrete inverse theory*. Academic Press, New York p 52
- Millot C (1990) The Gulf of Lions' hydrodynamics. *Continental Shelf Res* 10: 885–894
- Palma ED, Matano RP (1998) On implementation of passive open-boundary conditions for a general circulation model: the barotropic mode. *J Geophys Res* 103: 1319–1341

- Petrenko A (2003) Circulation features in the Gulf of Lions, NW Mediterranean Sea; importance of inertial currents. *Oceanolog Acta* 26: 323–338
- Seiler U (1993) Estimation of open-boundary conditions with the adjoint method. *J Geophys Res* 98: 22855–22870
- Talagrand O, Courtier P (1987) Variational assimilation of meteorological observations with adjoint vorticity equation. *Quart J Roy Meteorol Soc* 113: 1311–1328
- Weaver AT, Vialard J, Anderson DLT (2003) Three- and four-dimensional variational assimilation with a general circulation model of the tropical Pacific Ocean, part I. Formulation, internal diagnostics and consistency. *Monthly Weather Rev* 131: 1360–1378